Synaptic mechanisms modulate the spatiotemporal dynamics of striatal direct pathway neurons and motor output

John J Marshall[1,*], Jian Xu[1], Nai-Hsing Yeh[1], Seongsik Yun[1], Toshihiro Nomura[1], John N Armstrong[1], Jones G Parker[1,2,3,*], Anis Contractor[1, 2, 4,*]

[1]Department of Neuroscience, Feinberg School of Medicine, Northwestern University, Chicago IL 60611.

[2]Department of Psychiatry and Behavioral Sciences, Feinberg School of Medicine, Northwestern University, Chicago IL 60611.

[3]Department of Pharmacology, Feinberg School of Medicine, Northwestern University Chicago IL 60611.

[4]Department of Neurobiology, Weinberg School of Arts and Sciences, Northwestern University, Evanston IL 60201.

Correspondence: *John J Marshall
Dept of Neuroscience
Northwestern University Feinberg School of Medicine
303 E. Chicago Ave
Chicago, Il 60611
j-marshall@northwestern.edu
Tel: 312 503 0276

*Jones G Parker
Dept of Neuroscience
Northwestern University Feinberg School of Medicine
303 E. Chicago Ave
Chicago, Il 60611
Jones.parker@northwestern.edu
Tel: 312 503 3165

*Anis Contractor
Dept of Neuroscience
Northwestern University Feinberg School of Medicine
303 E. Chicago Ave
Chicago, Il 60611
Jones.parker@northwestern.edu
Tel: 312 503 3165

Words in Abstract – 159
Introduction – 896
Discussion - 1431
Number of Pages - 37
Number of Figures - 5

Abstract

Striatal spiny-projection neurons (SPNs) integrate glutamatergic inputs from the motor cortex and thalamus with neuromodulatory signals to regulate motor output. *In vivo* Ca^{2+} imaging has demonstrated that ensembles of direct and indirect pathway SPNs (dSPNs, iSPNs) are coactive during spontaneous movement. Co-activity is statistically greater among nearby neurons, correlates with behavioral state, and undergoes plasticity in an SPN-type-specific manner under pathological conditions. This spatially clustered co-activity could reflect shared excitatory inputs. However, whether and how synaptic mechanisms generate this distinctive spatiotemporal activity is unknown. Here, we show that the Group I metabotropic glutamate receptor 5 (mGluR5), which regulates synaptic strength at corticostriatal synapses, is a key mediator of spatially clustered SPN co-activity. Pharmacological modulation of mGluR5 signaling bidirectionally altered movement and spatially clustered dynamics, but not the absolute level of activity of dSPNs. Targeted deletion of mGluR5 in dSPNs recapitulated the effects on spatiotemporal neural dynamics and movement demonstrating a striatum-specific effect of mGluR5. Targeted deletion of mGluR5 also produced changes in the synaptic properties of dSPNs. These results show that properties of excitatory synapses influence motor function by shaping the characteristic spatially clustered patterns of co-activity that typify dSPN activation *in vivo*.

Introduction

The dorsal striatum is central to movement initiation and to regulating the kinematics of learned movements [1,2]. Synaptic plasticity in this input structure of the basal ganglia has been demonstrated to be important for motor learning [3]. In particular, the strength of corticostriatal synapses formed between the motor cortex and spiny-projection neurons (SPNs) in the dorsolateral striatum (DLS) are strengthened by learning a motor sequence [4] or during the acquisition of a new motor skill [5,6]. Glutamatergic, corticostriatal inputs form synapses onto two types of SPNs that are distinguished by their expression of dopamine receptor subtypes and downstream axonal projections.

The D1 dopamine receptor-expressing, or direct pathway SPNs (dSPNs) project monosynaptically to the output nuclei of the basal ganglia, the substantia nigra pars reticulata (SNr) and globus pallidus internal segment (GPi). By contrast, D2 dopamine receptor-expressing SPNs (iSPNs) project indirectly to basal ganglia output nuclei via the globus pallidus external segment (GPe) and the subthalamic nucleus (STN) [7]. In classical models of the basal ganglia circuit, activity in dSPNs facilitates movement and activity in iSPNs inhibits movement. Therefore, the relative level of activity between the two populations predicts an animal's motor state, for instance whether the animal is moving or at rest. This rate-model framework of striatal function garnered early support from anatomical and pharmacological observations as well as findings from studies investigating the neuropathology of striatum-related neurodegenerative disease [8].

However, the rate-model is inconsistent with more recent observations employing *in vivo* imaging techniques. In these studies, where the activity of genetically defined iSPNs and dSPNs can be monitored concurrently in awake behaving animals, dSPNs and iSPNs are consistently co-active during movement initiation and procession through movement sequences [9]. More recently, it was shown that dSPNs and iSPNs simultaneously activate with spatially clustered dynamics, and this spatiotemporal co-activity is important for motor control [10-12]. Spatiotemporal clustering, or heightened co-activity among proximal SPN pairs, is most pronounced during periods of rest as well as during transitions from rest to movement and subsides as SPNs become more active during movement progression [10-13]. Importantly, dopamine signaling appears to play an important role in sculpting these dynamics. The loss of dopamine diminishes the spatiotemporal coordination of iSPN activity, while heightened dopamine release de-correlates activity in dSPNs and heightens iSPN co-activity [10-13].

Although the exact mechanisms that constrain the spatiotemporal coordination of dSPN and iSPN activity are not known, SPNs have hyperpolarized resting membrane potentials that prevent action potential generation in the absence of glutamatergic input [14,15]. Given that glutamate is required for SPN activation, and given dopamine's role in modifying the strength of glutamatergic synapses in dSPN and iSPNs, it is likely that

synaptic plasticity influences the spatiotemporal dynamics of SPN activity by regulating their collective sensitivity to convergent excitatory inputs [16,17].

dSPNs and iSPNs receive excitatory input from both the cortex and thalamus. Cortico- and thalamostriatal synapses differ in their expression of pre- and post-synaptic neurotransmitter receptors and forms of synaptic plasticity[18]. In particular, extensive *in vitro* work has demonstrated various mechanistically distinct types of long-term potentiation (LTP) and long-term depression (LTD) at cortical inputs to dSPNs and iSPNs [19,20]. While the range of physiological and neuromodulatory mechanisms of corticostriatal plasticity are complex, one particularly well studied type of plasticity is endocannabinoid (eCB) dependent LTD, induced *in vitro* by moderate to high frequency stimulation of corticostriatal inputs paired with postsynaptic depolarization [18]. Importantly, corticostriatal LTD requires activation of postsynaptic Gq-linked, Group I metabotropic glutamate receptors (mGluRs). mGluR activation causes the mobilization of endocannabinoids (eCBs) from the postsynaptic neuron which act as a retrograde signal by activating presynaptic CB1 receptors reducing the release probability of glutamatergic corticostriatal synapses [21]. mGluR LTD of corticostriatal synapses occurs in both dSPNs and iSPNs [22] but not at thalamostriatal synapses [18]. eCB release and retrograde signaling can also produce transient modulation of presynaptic release causing short term depression of corticostriatal synapses [23,24] similar to what has been observed at synapses in several other brain regions [25]. Despite extensive *in vitro* work, little is known about the circumstances under which eCB-dependent synaptic modulation occurs *in vivo,* and therefore how it may relate to motor behavior. Moreover, it is unknown how modulation of corticostriatal synaptic strength regulates the level and/or spatiotemporal dynamics of SPN activity and how these synaptic changes relate to movement.

Given the prominent role of mGluR5 signaling in corticostriatal plasticity, we asked whether these receptors contribute to voluntary movement and the dynamics of dSPN activity in the DLS. We found that manipulating mGluR5 signaling had bidirectional effects on movement and the spatiotemporal dynamics of dSPN activity, with minimal effects on their overall levels of activity. Specifically, using *in vivo* Ca^{2+} imaging we

found that pharmacological inhibition of mGluR5 signaling produced a reduction in spontaneous movement and heightened the spatially clustered patterns of co-activity in dSPNs, whereas positive modulation of mGluR5 signaling had the opposite effects. Consistent with these findings, conditional knockout of mGluR5 in dSPNs (D1 cKO mice) had minimal effects on the levels of either dSPN or iSPN activity, but specifically increased the spatiotemporal coordination of dSPN activity and reduced spontaneous locomotion. Collectively, these findings suggest that synaptic plasticity mechanisms bidirectionally constrain the spatiotemporal coordination, but not the levels of dSPN activity, into states that correlate with increased or decreased locomotor activity. Our study lays the groundwork for dissociating the separable roles of the activity rates versus patterning of SPN activity in motor control and has implications for correcting any disruptions of this patterning in basal ganglia-associated diseases.

Results

dSPNs exhibit spatially clustered activity that varies with movement

There is a strong correlation between spatiotemporal patterns of SPN activity and motor output [10-12], but it is not known if synaptic properties modulate this coordinated activity *in vivo*. To assess the activity of dSPNs during spontaneous motor behavior, we implanted gradient refractive index (GRIN) lenses into the dorsolateral striatum of mice expressing Cre-recombinase in dSPNs under the control of the *Drd1a* promoter. A Cre dependent AAV to express GCaMP6f was introduced either by a prior stereotaxic injection of virus or by coating the lenses with a silk fibroin film containing the AAV (**Figure 1a**) [26]. The GRIN lens was coupled to a head-mounted miniscope for 1P imaging of somatic Ca^{2+} events[27]. **Figure 1b** shows an example of a field of view from one mouse and the segmented outlines of neurons after processing of the videos (*see* **Methods**) and examples of individual dSPN Ca^{2+} dynamics (**Figure 1c**). Consistent with prior observations [13], Ca^{2+} event rates in dSPNs increased during periods of movement (**Figure 1d, e**). The probability of a Ca^{2+} event in detected cells (defined as fluorescence change of 2.5× the baseline for each cell, *see* **Methods**) increased during movement (**Figure 1d**) and the Ca^{2+} event rate increased with increasing animal velocity (**Figure 1e**). Previous work has demonstrated that dSPNs and iSPNs are

spontaneously co-active in spatially intermingled clusters, a feature that has been proposed to be important for action selection [10-12,28]. To examine this spatiotemporal coordination and its modulation by movement state, we measured dSPN coactivity using a Jaccard index of dSPN pairs as a function of the Euclidean distance between them in the DLS. This measure captures co-activity between neuron pairs (as opposed to co-inactivity) more specifically than a linear correlation coefficient (**Figure 1f; Methods**) [11]. Across all cell pairs in the field-of-view for each session, a correlation matrix was generated in which, for each frame of the recording, the cell pair was scored a 1 if both cells were active, or 0 otherwise. These scores for each frame were divided by the number of events in both cells, to generate a co-activity score for that pair. **Figure 1f** shows schematized raster plots to demonstrate this process. Then, those values were normalized to averages measured from independently shuffled Ca^{2+} traces for each cell in the recording (using 1000 independent shuffles for each cell trace), to control for changes in mean activity level between conditions (**Figure 1f**). If cells were co-active independently of distance, then a plot of co-activity normalized to the shuffled data as a function of distance would be flat (**Figure 1g**). While clustered co-activity (*i.e.*, higher among proximal cells) would show a downward sloping curve (**Figure 1h**). Consistent with prior reports [10-12], this analysis revealed that co-activity among neuron pairs is markedly higher among proximal cells and decreases with increasing Euclidean distance between pairs (**Figure 1i**). Furthermore, as we had previously demonstrated, co-activity among all pairs was higher during rest and decreased during periods of movement (**Figure 1j**) [13].

The spatiotemporal dynamics of dSPN activity is modulated by mGluR5

The dominant form of synaptic plasticity at corticostriatal synapses is mediated by Grp1 mGluRs [18] and the primary receptor of this class expressed in SPNs is mGluR5 [29]. Germline deletion of mGluR5 causes significant motor phenotypes, but it is not known how mGluR5 signaling directly affects motor function [30]. Due to the known importance of mGluR5 in modulating synaptic weight at corticostriatal synapses, we hypothesized that pharmacological modulation of mGluR5 would affect SPN dynamics in vivo.

To assess the effects of modulating mGluR5 activity on dSPN dynamics during spontaneous behavior, we injected mice with vehicle or the mGluR5 negative allosteric modulator (NAM) fenobam (26 mg/kg via i.p. injection) immediately prior to a 60-minute open field test. We analyzed dSPN activity from 8 animals expressing GCaMP6f in dSPNs and implanted with GRIN lenses in the DLS (**Figure2a–c**). We measured activity as mice spontaneously explored an open field arena. On average we recorded from 91 dSPNs per mouse in these experiments.

Fenobam treatment uniformly reduced locomotion (**Figure 2d, e**), an effect that was driven more by a reduction in movement bout duration than the frequency of movement bouts (**Figure 2f**). Interestingly, dSPN event rates were unchanged following fenobam injection, with Ca^{2+} event rates in dSPNs increasing with spontaneous locomotor speed across the range of running speeds in both fenobam and vehicle injected animals (**Figure 2g**).

However, fenobam treatment significantly increased the pairwise co-activity of dSPNs across the whole range of cell-cell distances (**Figure 2h-i**). As fenobam treatment reduced movement, and co-activity is modulated by movement, we further analyzed changes during periods of movement and rest. While fenobam treatment increased dSPN co-activity during both periods of rest and movement, its effects were most pronounced during periods of rest (**Figure 2j, k**). Normalizing the levels of co-activity in proximal bins to the values at rest for each mouse showed that, fenobam did not affect the relative decrease in co-activity between periods of rest and movement (**Figure 2i**).Taken together these results suggest that fenobam may suppress movement by transitioning spatiotemporal dSPN ensemble dynamics towards a rest-associated state without affecting the absolute rates of their activity.

A positive allosteric modulator (PAM) of mGluR5 increases movement and decreases SPN co-activity

Next we sought to determine how administration of an mGluR5 PAM affects motor output and SPN dynamics. We selected JNJ-46778212/VU0409551 (JNJ) an mGluR5 PAM with demonstrated *in vivo* efficacy and known pharmacokinetics in mice [31]. We administered JNJ (100 mg/kg) or vehicle via i.p. injection 30 minutes prior to measuring

dSPN dynamics during one-hour of locomotion in an open field arena. In contrast to fenobam, JNJ treatment decreased the amount of time the animal spent at rest (**Figure 3a**) increased locomotor speed (**Figure 3b**) and increased the duration but not frequency of movement bouts (**Figure 3c, d**). Like fenobam, JNJ did not significantly affect the levels of dSPN activity when measured as a function of the animal's running speed (**Figure 3e**). However, JNJ significantly decreased the co-activity among dSPN cell pairs measured across a range of Euclidean distances (**Figure 3f–h**). This effect was most pronounced during periods of rest (**Figure 3i, j**). Therefore, JNJ treatment had effects that were qualitatively the inverse to the effects of fenobam on locomotion and dSPN activity. These findings are consistent with the idea that JNJ promoted movement by inducing movement-associated dSPN ensemble dynamics by de-correlating their activity.

mGluR5 activation in the striatum results in the mobilization of eCBs, specifically 2-AG in dSPNs[21,23-25]. Therefore, we asked whether enhancing eCB levels by preventing 2-AG degradation using the monoacylglycerol lipase (MAGL) inhibitor JZL-184 affected the spatiotemporal dynamics of dSPN activity. We administered mice with JZL-184 (10 mg/kg) intraperitoneally before recording dSPN Ca^{2+} activity for 60 minutes in an open field arena. Interestingly, in contrast to the mGluR5 PAM, JZL-184 significantly reduced rate of Ca^{2+} events (**Figure 3k**) but did not affect the co-activity of dSPNs (**Figure 3l**). These results suggest that broadly enhancing eCB levels does not recapitulate the effects of potentiating mGluR5 signaling specifically.

Collectively these results demonstrate that potentiating mGluR5 signaling shifts dSPN dynamics to a less correlated state, while inhibiting mGluR5 signaling enhances the correlated state of dSPNs. It is notable that spontaneous dSPN activity is less correlated during periods of movement than rest, and de-correlated dSPN activity has been shown to occur in hyperkinetic states (*e.g.*, dyskinetic and hyperdopaminergic states [11,13]). These observations suggest that mGluR5 signaling suppresses movement by altering the strength of excitatory synapses in dSPNs and their co-recruitment via excitatory afferents.

mGluR5 reduces corticostriatal glutamatergic transmission at dSPN synapses in the dorsolateral striatum

Our experiments demonstrated changes in striatal dSPN network activity that correlate with changes in motor behavior mediated by pharmacologically modulating mGluR5. To determine whether modulating mGluR5 specifically in striatal dSPNs mediates the observed effects on locomotor and striatal activity, we used a genetic approach to selectively manipulate mGluR5 in D1 receptor-expressing neurons. To do this, we crossed *Grm5*$^{fl/fl}$ mice [32] to D1-Cre mice [33] to create conditional knockout mice (D1 cKO) mice. Further crossing with a Cre reporter allele (Ai9) [34] enabled us to perform patch-clamp recordings from visually identified dSPNs in striatal slices to record corticostriatal EPSCs (**Figure 4a**). As we have previously demonstrated [24], a ten minute application of the group 1 mGluR agonist DHPG (100 µM) caused a depression of EPSCs in WT recordings (**Figure 4b**). This effect was significantly diminished in recordings from cKO mice, demonstrating a disruption of mGluR5 signaling in cKO mice (**Figure 4c**).

A number of behavioral phenotypes have been described in mice with constitutive, germline *Grm5* deletion [30]. Given our previous observations and the fact that SPN activity in the dorsal striatum is important for motor control, we assessed whether selective ablation of *Grm5* in dSPNs affected locomotion and motor learning. Tracking distance travelled in an open field we found that the D1 cKO mice had reduced spontaneous locomotion (**Figure 4d**) and displayed a reduction in total distance travelled (**Figure 4e**). We also found the D1 cKO mice had diminished digging behavior in a novel environment (**Figure 4f**). Taken together these results demonstrate that selectively disrupting mGluR5 signaling in dSPNs reduces spontaneous movement in novel environments.

To measure locomotion in the home cage setting, we introduced running wheels and monitored activity over 7 days. During the first 3 days, D1 cKO mice demonstrated significantly reduced voluntary running (**Figure 4h & i**). However, both control and D1 cKO mice increased the time spent running over the course of 7 days such that the difference between the groups was not significant by day 7 (**Figure 4i**).

Finally, on an accelerating rotarod D1 cKO mice showed a consistently reduced latency to fall over the course of 12 training trials across three days (**Figure 4g**). Despite this deficit, D1 cKO mice did improve over the course of training, indicating that they were capable of learning the task. Thus, the D1 cKO mice exhibited a primary deficit in spontaneous motor activity with only minor deficits in the learned motor tasks of running on a wheel or forced locomotion on the rotarod.

Because of the clear motor phenotype in D1 cKO mice we first measured whether there were any changes in the intrinsic or synaptic properties of dSPNs in these mice. Whole cell current clamp recordings from visually identified dSPNs expressing tdTomato found no difference in the voltage response to increasing current injection suggesting no alteration in the intrinsic excitability of dSPNs in D1 cKO mice (**Figure 4j, k**). In recordings of mEPSCs that reflect all excitatory synapses (corticostriatal and thalamostriatal), we found that the amplitudes of mEPSCs were unchanged, but their frequency was significantly increased in dSPNs from D1 cKO mice (**Figure 4l–m**), indicating increased release probability when mGluR5 expression is disrupted.

Spatiotemporal activity of dSPNs is disrupted in D1 cKO mice

To measure the *in vivo* dynamics of dSPNs in D1 cKO mice, we implanted GRIN lenses into the DLS of control and D1 cKO mice and analyzed dSPN Ca^{2+} activity during 20 minutes of open field exploration (**Figure 5a – e**). Consistent with our previous results, the event rate of dSPN Ca^{2+} transients increased with locomotor speed in both experimental and control mice (**Figure 5d**). Selective mGluR5 deletion in Drd1a-expressing neurons did not alter the rate of dSPN Ca^{2+} events compared to control mice (**Figure 5d**). Instead, the normalized coactivity of dSPNs (analyzed across 50-μm bins of pairwise cell distances) was significantly increased in D1R cKO mice, similar to the effect of the mGluR5 NAM fenobam (**Figure 5e**). Therefore, targeted genetic deletion of mGluR5 in dSPNs had qualitatively similar effects as systemic administration of the mGluR5 NAM on the spatially clustered dynamics of dSPNs.

Finally, because both dSPNs and iSPNs exhibit spatially clustered activity *in vivo*, and because they are synaptically connected through recurrent collaterals with stronger unidirectional iSPNs to dSPNs coupling [35], it is possible that disruption of mGluR5

signaling in dSPNs may also affect the levels and spatiotemporal dynamics of activity in intermingled iSPNs. To address this question, we used a viral “Cre-off” strategy to express GCaMP6 in Cre-negative, iSPNs of *Drd1a*-Cre; *Grm5*$^{fl/fl}$ mice[36]. We found that the deletion of mGluR5 in dSPNs had no effects on either the levels of activity in iSPNs (**Figure 5f**) or the spatiotemporal clustering (**Figure 5g**). Therefore, the alteration in SPN dynamics in D1 cKO mice appear to be cell autonomous as specific targettijng of mGluR5 in dSPNs does not affect iSPN activity in D1 cKO mice.

Together these results demonstrate that the manipulation of mGluR5 signaling, through pharmacological or targeted genetic means, leads to changes in the spatiotemporal patterns of activity in dSPNs with minimal effects on their overall levels of activity. Notably, these spatiotemporal dynamics varied with locomotor speed under normal conditions, and manipulations of mGluR5 signaling induced changes in these dynamics that correlated with locomotor state. These findings suggest that these two facets of activity—levels and spatiotemporal patterning of activity—are separable and provide important insights into the role of spatiotemporally coordinated activity in the generation of movement.

Discussion

The rate-model of basal ganglia function posits that activity in dSPNs and iSPNs have distinct and opposing effects on movement. This framework is primarily based on anatomical evidence from the distinct projection targets of dSPNs and iSPNs and electrophysiological recordings in their downstream projection targets under conditions modeling parkinsonism [8]. These target nuclei inhibit motor control nuclei in the hindbrain mesencephalic locomotor region and thalamic regions that project to the motor cortex [37,38]. In this context, dSPN activation is predicted to increase activity in these motor control regions to facilitate movement, while iSPN activation is predicted to decrease activity in these same regions to inhibit movement.

However, this classical model is not supported by recent *in vivo* imaging studies using fiber photometry or endoscopy to record Ca^{2+} activity in genetically specified dSPNs or iSPNs. In contrast to the predictions of the rate-model, dSPNs and iSPNs are indistinguishably responsive to increases and decreases in movement [9]. Intriguingly, *in*

vivo endoscopy has shown that overlapping clusters of dSPNs and iSPNs co-activate during movement, with small but statistical correlations between the activation of different clusters during different movement types [10]. These findings suggest an alternative model where, in contrast to the relative level of activity in each SPN type, the spatial patterning of co-activity among SPNs may be important for specifying proper motor output.

Despite the evidence that SPNs may influence movement via the coordination of their activity, the biological mechanisms responsible for these coordinated patterns are not known. Seminal *in vitro* electrophysiology studies demonstrated that SPNs fire action potentials coincident with large excitatory inputs that shift their resting membrane potential to transiently stable, depolarized "up" states [14,15]. These excitatory inputs arise from the cortex and thalamus. Our results suggest that the modulation of the synaptic weight, particularly at corticostriatal synapses where several forms of plasticity require mGluR5 receptors, is a crucial mechanism constraining the patterns of dSPN co-activity in states associated with movement or rest.

Spontaneous motor output correlates with the level of coactivity in dSPNs

In the current work, we have used pharmacological and genetic manipulations to examine how activity in dSPNs varies with movement while targeting the receptor controlling the dominant form of synaptic plasticity in the DLS. Systemic administration of the mGluR5 negative allosteric modulator, fenobam, led to significant increases in co-activity among dSPNs and reduced locomotor activity. By contrast, systemic administration of the mGluR5 positive allosteric modulator JNJ led to decreased co-activity and increased locomotion. Notably, neither pharmacological manipulation of mGluR5 led to significant changes in the rate of dSPN Ca^{2+} events. Our results suggest a model whereby either potentiating or inhibiting mGluR5 signaling alters the recruitment of dSPNs such that the overall activity level is preserved but that the patterns of their co-activity change in a manner that corresponds to motor output. This is further confirmed by our data from animals with targeted deletion of mGluR5 in dSPNs, which similarly showed no change in event rate but an increase in co-activity.

Our results are consistent with prior analysis demonstrating that the co-activity among pairs of dSPNs is higher at rest and decreases during movement [13]. Here we found that pharmacological manipulations that alter these clustered co-activity states correspondingly alter the levels of spontaneous motor output. Specifically, shifting the dSPN network to a level of higher co-activity, as with fenobam treatment or mGluR5 deletion in dSPNs, leads to a reduction in the amount of time animals spent moving. By contrast, potentiating mGluR5 receptors with systemic JNJ administration led to an increase in time spent moving and a corresponding decrease in the co-activity of dSPNs.

Our *ex vivo* electrophysiology data from cKO animals further supports these conclusions, as disrupting endogenous mGluR5 signaling in dSPNs does not result in changes in the excitability of neurons. Instead, genetic deletion of mGluR5 altered the synaptic properties of dSPNs, likely an adaptive response consistent with the established role of mGluR5 in regulating corticostriatal synaptic weights. These findings suggest that these selective changes in synaptic plasticity may underlie the altered spatiotemporal patterning of dSPN activity without changes in their overall levels of activity observed *in vivo*.

In vitro studies have demonstrated that mGluR5 activation occurs following pairing of postsynaptic depolarization with moderate to high frequency excitatory synaptic input [21]. mGluR5 activation can result in the long term depression (LTD) of synaptic transmission or a more transient depression in release probability [23,24,39]. Our results link the regulation of synaptic weights by mGluR5 to the coordinated activity of dSPN *in vivo.*

Global enhancement of eCB levels does not alter clustered co-activity

The lack of change in spatiotemporal coordination following systemic administration of the 2-AG degradation inhibitor JZL-184 suggests that global enhancement of eCB levels does not produce a similar outcome as modulating mGluR5 signaling. However, in contrast to selective mGluR5 modulation we did observe a reduction on overall dSPN event rates with JZL. One possibility is that a degree of synaptic specificity is required to affect clustered activation of dSPNs. Thus, JZL treatment may have exerted such broad effects on the circuit that it resulted in a different outcome for neural clustering and

motor output than that observed following treatment with the allosteric modulators of mGluR5 receptors that modify synaptic weight.

These results support a model whereby the level of co-activity among specific groups of dSPNs is potentially important for controlling motor output. Therefore, globally altering the synaptic weights of all neurons may overshadow the results of synaptic alterations in specific subsets of SPNs. This idea is consistent with the notion that individual dSPNs may be precisely tuned to have specific roles in regulating motor output, such that altering the activity of one dSPN subgroup would not have the same effect as altering the activity of a different sub-group. This interpretation is also at odds with the classical rate-dependent models of SPN activity.

Role of non-dSPN mGluR5 receptors in regulating movement

There are notable differences in the design of our experiments using conditional deletion of mGluR5 from dSPNs and systemic administration of a negative allosteric modulator of mGluR5. Following fenobam administration, we observed a significant increase in co-activity when animals were at rest and a smaller increase during movement. Additional experiments are necessary to determine if this is also the case in dSPNs from cKO animals, but this could provide insights into the specific role of mGluR5 in dSPNs compared to its role in other cell types or brain regions affected by systemic fenobam treatment.

Within the striatum alone, mGluR5 is expressed in iSPNs and interneurons and modulation of these cell types by systemically administered compounds could produce changes in behavior and striatal circuit function. dSPNs receive GABAergic input from both iSPNs as well as striatal interneurons. Of particular note, parvalbumin-positive fast-spiking interneurons also receive excitatory input from the cortex and provide feedforward inhibition onto both subtypes of SPNs, and genetic disruption of mGluR5 in parvalbumin interneurons increases striatum-dependent repetitive behaviors [40]. The modulation of synaptic strength at these connections by fenobam and JNJ could also partly account for the effects of these compounds on dSPN activity and behavior when systemically administered, which would not occur in cKO animals.

Collateral inhibition between SPNs is another potential source for modulation of co-activity. *In vitro* electrophysiology has shown that dSPNs are more likely to form synapses onto other dSPNs, while iSPNs form synapses onto neurons of both pathways with equal probability [35]. However, the strength of collateral synapses formed by dSPNs appears to be smaller than that of synapses formed by iSPNs. Our analysis of iSPN activity in cKO mice suggests that iSPN circuit properties are largely normal when mGluR5 is genetically disrupted in dSPNs, perhaps reflecting the less substantial modulation of iSPN circuitry by dSPNs reported in the striatum, at least during spontaneous behavior. Whether this relationship holds across additional behavioral states remains to be addressed. Additionally, whether disruption of iSPN networks affects dSPN networks, perhaps due to stronger unidirectional iSPN-dSPN connectivity, is a key question for further research.

Translation implications of dSPN spatiotemporal dynamics

The relationship of mGluR5 pharmacology to dSPN spatial coordination and motor output is also clinically relevant to the treatment of motor disorders. Prior studies examining the spatial coordination of SPNs in parkinsonian mice demonstrated that, following dopamine depletion to model the parkinsonian state, dSPN activity was reduced but maintained spatial coordination [11]. However, when levodopa induced dyskinesia (LID) was modelled in these animals, dSPNs lost spatial coordination. In the current work, we show that pharmacological inhibition of mGluR5 increases spatial coordination. It is tempting to speculate, therefore, that in the case of LID, the therapeutic efficacy of mGluR5 NAMs may involve regulation of the spatially coordinated co-activity of dSPNs. Additionally, further examination of how spatially coordinated SPN activity is disrupted in motor diseases involving basal ganglia pathology, may be a promising avenue for guiding future therapeutic development.

In summary our data demonstrate that the modulation of signaling that affects synaptic properties of excitatory synapses onto dSPNs is a key mediator of the normal patterns of SPN co-activity that typify the striatum's neural ensemble dynamics in relation to spontaneous movement. These results provide further support for models where the local synchronization of SPNs (and the basal ganglia circuit in general) is a stronger

determinant of motor output in than their overall levels of activity. Our results also provide a framework for future lines of inquiry to address how striatal synaptic properties shape circuit function and striatum-dependent behavior.

Methods:

Mice

Animals were group housed with 14-hr:10-hr Light/Dark cycle and food and water were provided ad libitum. Mice of both sexes, between 4-12 months old, were used and all experiments were performed in accordance with procedures approved by the Northwestern University IACUC. To express GCaMP6f in dSPNs we used mice expressing Cre recombinase under the control of the drd1a promoter (D1cre) [41]. A Cre-dependent GCaMP6f under the control of the synapsin promoter (pAAV.Syn.Flex.GCaMP6f.WPRE.SV40, 100833-AAV9 from Addgene) was used for delivery of the construct. For in vitro patch clamp electrophysiology experiments we further crossed the D1Cre line to mice expressing a Cre-dependent tdTomato reporter inserted in the *Gt26Sor* (Rosa26) locus (Ai9), in order to identify dSPNs in the DLS [42]. For genetic deletion of mGluR5 we used floxed mGluR5 mice ($mGluR5^{loxP/loxP}$) [32] crossed to either D1cre mice (D1cre; $mGluR5^{f/f}$) for in vivo imaging experiments, or D1 cre mice crossed with Ai9 mice (D1cre; $mGluR5^{f/f}$; $Ai9^{+/+}$) for patch clamp experiments. All mice were maintained on the C57BL6/J background strain.

Behavioral analysis

Motor learning on the accelerating rotarod:

Mice of both sexes were placed on the rotarod and the initial revolution speed set to 4 rpm for 120 s. The rotarod then accelerated at a rate of 0.12 $rpm \cdot s^{-1}$ for 300 s. Mice were trained in three trials per day with a 30 min inter-trial interval for four consecutive days (12 trials total).

Open Field:

The dimensions of the square open field arena (in cm) were 60 l × 60 w × 30 h . Animals were placed in the middle of the arena at the start of the test and remained in

the arena for 30 min during which time their position was tracked using an overhead camera and analyzed using software (Limelight; Actimetrics).

Digging behavior:

Mice were placed in a novel cage containing wood chip bedding (3-cm deep) in a brightly lit, open area. Animals remained in the testing cage for 15 min. Mouse digging time was manually scored using a stopwatch.

Voluntary Wheel Running:

Mice of either sex were single-housed with wireless running wheels (MedAssociates) for at least 7 days. Total distance run was quantified for each day.

Virus Injection:

For mice that received a viral injection (pAAV.Syn.Flex.GCaMP6f.WPRE.SV40, 100833-AAV9 from Addgene) prior to GRIN lens implant, we anesthetized mice with isoflurane (2% in O_2) and stereotaxically injected virus at a rate of 250 nl min^{-1} into the DLS using a microsyringe with a 28-gauge beveled-tip needle (Hamilton Company, Reno, NV). Stock titer virus was diluted 1:10 with sterile PBS. The coordinates for injection were: A/P +/- 0.05 mm, M/L +/- 1.8 mm, D/V -2.4mm (from dura). For all DV coordinates, we went 0.1 mm past the injection target and then withdrew the syringe back to the target for the injection. After each injection, we left the syringe in place for 10 minutes and then slowly withdrew the syringe. We then sutured the scalp, injected analgesic (Buprenorphine SR, 1 mg kg^{-1}), as well as meloxicam (2x / day for 48 hours, 5 mg·kg^{-1}), and allowed the mice to recover for at least 14 days.

Silk fibroin coating of GRIN lenses:

For animals in which we implanted a GRIN lens coated with a fibroin:AAV mixture, we autoclaved both GRIN lenses, and a small aliquot of 5% W/V silk fibroin solution, prior to coating. Then, the sterile fibroin solution was mixed 1:1 with stock titer AAV (pAAV.Syn.Flex.GCaMP6f.WPRE.SV40, 100833-AAV9 from Addgene). A microsyringe with a 23 gauge flat tip needle (Hamilton Company, Reno, NV) with a manual stereotaxic injector (Stoelting) was used to apply a 1µL droplet of the mixture to the tip

of the GRIN lens in a biological safety cabinet. The mixture was allowed to dry slightly for 5 minutes with the droplet in contact with both the GRIN lens surface and the syringe needle tip before the syringe needle was removed, this prevented the mixture from coating the side of the lens. Once the needle was removed the droplet was allowed to fully dry to the surface of the lens for at least 1 hour before implanting. Lenses were stored at 4°C for implanting either the same day or within approximately 24 hours.

Surgical implantation of GRIN lens and viral transduction:

Mice were anesthetized with isoflurane in O_2 (induction 4%; maintenance 2–3%). Following verification of anesthesia, hair was trimmed from the incision site, the scalp cleaned with three alternating swabs of betadine and 70% ethanol, and an incision made through the scalp to uncover the skull. The skull surface was cleaned and verified to be level by measuring the coordinates of bregma, lambda, and two sites +/- 2mm lateral to the midline. The M/L and A/P coordinates for implantation of the GRIN lens were marked on the skull (A/P +/- 0.05 mm, M/L +/- 2 mm) and a Dremel with a sterilized 0.6-mm tip was used to remove an approximately 2-mm circular region around the implant site. The skull was cleaned, dried, and scored crosswise with a scalpel. While continuously perfusing the tissue with ACSF, the dura and cortex were removed using a 26 GA blunt-end needle connected to a vacuum line until the fibers of the corpus callosum became visible, at which point a 30 GA blunt-end needle was used to carefully remove the fibers of the callosum until striatal tissue became visible under a dissecting microscope. A 1-mm or 1.8-mm diameter GRIN lens was then lowered into the aspiration site (D/V -2.4 mm), held in place using a pipette tip and vacuum line attached to the stereotax. The lens was secured to the skull using dental cement (Metabond) and cyanoacrylate glue. Buprenorphine SR, (1 $mg \cdot kg^{-1}$) was administered following surgery, as well as meloxicam (2x / day for 48 hours, 5 $mg \cdot kg^{-1}$), dexamethasone (1x / day, 0.2 $mg \cdot kg^{-1}$ for 7 days), and Sulfatrim (for 7 days in the drinking water). Mice were allowed to recover for 2–4 weeks before mounting the miniature microscope.

Miniscope Mounting and Imaging:

Two-to-four weeks following surgery to implant the GRIN lens, the mouse was again anesthetized under the stereotax and a miniscope (UCLA V3 or V4) with a baseplate attached was lowered to the top focal plane of the GRIN lens. Once the optimal imaging plane was found, the baseplate was secured with dental cement (Metabond, Parkell).

In vivo Ca^{2+} imaging and Analysis:

All mice were habituated to the weight of the miniscope over a 60-minute session in the open field. Following habituation, we placed mice in the open field for 60 minutes each day for 1-3 days with the miniscope attached. For analysis of calcium dynamics in dSPN cKO mice, we analyzed data from the first 20 minutes of day 1 of these sessions. In the majority of animals used in these experiments, we used v3 miniscopes which required higher LED intensities compared to v4 miniscopes. Therefore, we limited recording to 20 minutes to limit photobleaching. For experiments testing fenobam, JZL and JNJ, 60 minutes of open field activity were recorded following IP injection. For these experiments we used v4 scopes which allowed for the use of lower LED intensities. Fenobam (26 mg/kg) and JZL (10 mg/kg) were administered immediately prior to the test, following a 15-minute habituation. Due to its pharmacokinetics, JNJ was administered 30 minutes prior to beginning the test. Fenobam was diluted in 40% beta-cyclodextrin, 10% DMSO, JZL and JNJ were diluted in 10% DMSO and 90% corn oil.

We used open source V3 and V4 miniscopes (https://github.com/Aharoni-Lab/Miniscope-v4) that were connected to a coaxial cable which connected to a miniscope data acquisition board (DAQ) 3.3. The DAQ was connected to a computer via a USB 3.0 cable. Data was collected via the Miniscope QT Software (https://github.com/Aharoni-Lab/Miniscope-DAQ-QT-Software) at 20 frames per second. Simultaneous video recordings of behavior were performed at approximately 30 fps, and data was aligned posthoc using the time stamps collected by the miniscope software for each frame. Miniscopes and DAQ boards were purchased from Open Ephys, LabMaker, or parts were machined by Shylo Steitler (UCLA) and assembled.

Pre-processing and motion correction:

Videos were preprocessed to remove sensor noise using a 2D FFT spatial frequency filter and lowpass butterworth filter (https://github.com/Aharoni-Lab/Miniscope-v4/tree/master/Miniscope-v4-Denoising-Notebook) and then motion correction was performed using the normcorr algorithm in the CaImAn package [43].

Identification of neurons (CNMF-E):

Cells were automatically identified using the CNMF-E algorithm [44]. Recordings were grouped in batches of 1-5000 frames for processing, and spatially downsampled 2x during running of the CNMF-E algorithm. The maximum neuron diameter was determined based on manual observation of each of the motion corrected videos in ImageJ and the minimum local correlation value (Cn) and signal to noise ratio (SNR) for a pixel to be used as a cell "seed" was determined by visualizing the correlation image for a subset of recording frames of each video. The threshold for merging neurons was set at 0.65, neurons were merged if their distances were smaller than two pixels and they had highly correlated spatial shapes (correlation >0.8) and small temporal correlations (correlation <0.4). The output of the CNMF-E analysis performed on the video was then manually checked to ensure accuracy.

Analysis of Ca^{2+} activity:

The cell Ca^{2+} activity traces from CNMF-E were processed first by scaling to the 99-percentile value of each cell's activity trace during the recording session. The resulting normalized trace was then expressed as a Z-score by subtracting each sample from the mean and dividing by the standard deviation of the entire trace. Finally, this trace was downsampled to 5Hz (using the maximum value within the down sampled regions) and this result was used for further analysis.

Ca^{2+} event rate and correlation to velocity:

A threshold crossing algorithm was used to detect peaks that were ≥2.5 s.d. above the baseline signal value for 1 second and the time of each event was calculated as the midpoint between the maximum value of the event and the preceding minimum [11]. We used EZ track [45] to compute the frame by frame velocity of the animal in the openfield

arena. Using custom Python scripts we applied a 1 second median filter to this velocity trace and downsampled to 5Hz for alignment to the Ca^{2+} activity data.

Pairwise cell co-activity:

The Jaccard index of pairwise coactivity was calculated following 1 second "forward-smoothing" of the Ca^{2+} activity traces as described previously [11]. The mean value of the Jaccard index was calculated as a function of the Euclidean distance between cells in a neuron pair and the mean values were binned into either 50 or 250 µm bins. These values were normalized to shuffled data sets where the Ca^{2+} traces for each cell were shuffled in time, using 1,000 independent shuffles of the binarized Ca^{2+} event traces for each cell. This data was used for statistical comparison of coactivity between groups as a function of distance, and behavioral state, i.e. moving or resting.

Slice procedure and in vitro Electrophysiological Recording:

Parasagittal slices containing the dorsal striatum were prepared using standard techniques. Mice were deeply anesthetized (xylazine 10mg/kg and ketamine 100mg/kg i.p.) before undergoing transcardial perfusion with an ice-cold sucrose artificial cerebrospinal fluid (ACSF) solution containing (in mM): 85 NaCl, 2.5 KCl, 1.25 NaH_2PO_4, 25 $NaHCO_3$, 25 glucose, 75 sucrose, 0.5 $CaCl_2$ and 4 $MgCl_2$, equilibrated with 95% O_2 and 5% CO_2. The brain was removed and mounted on the stage of vibratome (Leica Microsystems, Inc). 350 µm thick sections were made in ice-cold sucrose ACSF. Slices were transferred to a recovery chamber containing the sucrose slicing ACSF solution, which was gradually exchanged for a normal ACSF containing (in mM): 125 NaCl, 2.4 KCl, 1.2 Na_2PO_4, 25 $NaHCO_3$, 25 glucose, 1 $CaCl_2$ and 2 $MgCl_2$, while the slices were maintained at 30°C. Individual slices were transferred to a recording chamber and visualized under DIC. Micro-Manager open source software was used for collecting the CCD camera image [46]. For extracellular recordings, slices were perfused with normal ACSF containing (in mM): 125 NaCl, 2.4 KCl, 1.2 Na_2PO_4, 25 $NaHCO_3$, 25 glucose, 2 $CaCl_2$ and 1 $MgCl_2$. Recording electrodes were manufactured from borosilicate glass pipettes and had resistances of 3-5 MΩ when filled with regular ACSF. For whole-cell voltage clamp experiments, recording electrodes were filled with internal solution containing (in mM) 95 CsF, 25 CsCl, 10 Cs-HEPES, 10 Cs-EGTA, 2

NaCl, 2 Mg-ATP, 10 QX-314, 5 TEA-Cl, 5 4-AP for recording of EPSCs, or 75 $CsCH_3SO_3$, 60 CsCl, 1 $MgCl_2$, 0.2 EGTA, 10 HEPES, 2 Mg-ATP 0.3 GTP-Na_2, 10 Na_2-phosphocreatine,10 TEA, 5 QX-314. Striatal projection neurons (SPNs) were visually identified and were voltage clamped at -80mV. Miniature events (mEPSCs) were recorded in the presence of the Na^+ channel blocker TTX (1µM) and bicuculline (10 µM). Analysis of mEPSCs was performed using Eventer software (https://eventerneuro.netlify.app/).

Histology:

Following in vivo imaging experiments, mice were anesthetized using ketamine/xylazine and perfused with PBS containing 0.02% sodium nitrite and 4 mM $MgSO_4$ followed by 2% paraformaldehyde in 0.1 M sodium acetate buffer (pH 6.5) for 6 min, and 2% paraformaldehyde in 0.1 M sodium borate buffer (pH 8.5) for 12–18 min. The brains were removed from the skull, post-fixed overnight in 2% paraformaldehyde in 0.1 M sodium borate buffer (pH 8.5), then sectioned coronally at 50 µm on a Leica Vibratome VT1000s in PBS. The sections were collected and stored at 4 °C in PBS containing 0.02% sodium azide. Free-floating sections were rinsed for 30 min in PBS followed by four 15-min washes in PBS containing 0.1% Triton X-100 (Sigma, T8787) and 0.1% bovine serum albumin (BSA; Sigma, A4503). The sections were then blocked with 3% normal donkey serum (NDS; Jackson ImmunoResearch, 017-000-121) for 1 h and then incubated in primary antibody overnight (Mouse anti-GFP, Millipore, MAB3580). Sections were washed three times for 15 min and then incubated in secondary antibody for 1 h and washed three times prior to mounting and imaging with a 20× objective on a Nikon A1 confocal microscope. Z-series were taken with a 0.82 µm step size.

Statistics:

For comparisons of single mean values per mouse, for instance mean velocity per animal, we used non-parametric Mann Whitney U test or the Wilcoxon Signed Rank test. Where the same measurement was made multiple times, we used a repeated measures ANOVA. For cases where multiple different but correlated, non-independent, comparisons were made within mice, for instance in comparing mean event rates at different speeds or mean coactivity across neuron pairs at difference distances, we

used a linear mixed effects model (LMM) to account for the non-independence of measurements made from the same animal. The model was implemented using the statsmodels python package (https://www.statsmodels.org), the drug treatment or genotype was the independent variable, mean values measured per mouse are the dependent variables and individual mice are the group term. Where this model was used, we tested for the effect of genotype or drug treatment, and reported the significance for that measurement. In all figures, individual data points represent the mean of a group, and errors bars the standard error of the mean. N numbers for each group are specified in the figure legend.

References

1. Klaus, A., Alves da Silva, J., and Costa, R.M. (2019). What, If, and When to Move: Basal Ganglia Circuits and Self-Paced Action Initiation. Annu Rev Neurosci *42*, 459-483. 10.1146/annurev-neuro-072116-031033.
2. Wolff, S.B.E., Ko, R., and Olveczky, B.P. (2022). Distinct roles for motor cortical and thalamic inputs to striatum during motor skill learning and execution. Sci Adv *8*, eabk0231. 10.1126/sciadv.abk0231.
3. Dang, M.T., Yokoi, F., Yin, H.H., Lovinger, D.M., Wang, Y., and Li, Y. (2006). Disrupted motor learning and long-term synaptic plasticity in mice lacking NMDAR1 in the striatum. Proc Natl Acad Sci U S A *103*, 15254-15259. 10.1073/pnas.0601758103.
4. Rothwell, P.E., Hayton, S.J., Sun, G.L., Fuccillo, M.V., Lim, B.K., and Malenka, R.C. (2015). Input- and Output-Specific Regulation of Serial Order Performance by Corticostriatal Circuits. Neuron *88*, 345-356. 10.1016/j.neuron.2015.09.035.
5. Yin, H.H., Mulcare, S.P., Hilario, M.R., Clouse, E., Holloway, T., Davis, M.I., Hansson, A.C., Lovinger, D.M., and Costa, R.M. (2009). Dynamic reorganization of striatal circuits during the acquisition and consolidation of a skill. Nat Neurosci *12*, 333-341. 10.1038/nn.2261.
6. Hwang, F.J., Roth, R.H., Wu, Y.W., Sun, Y., Kwon, D.K., Liu, Y., and Ding, J.B. (2022). Motor learning selectively strengthens cortical and striatal synapses of motor engram neurons. Neuron *110*, 2790-2801 e2795. 10.1016/j.neuron.2022.06.006.
7. Gerfen, C.R., and Surmeier, D.J. (2011). Modulation of striatal projection systems by dopamine. Annu Rev Neurosci *34*, 441-466. 10.1146/annurev-neuro-061010-113641.
8. Nelson, A.B., and Kreitzer, A.C. (2014). Reassessing models of basal ganglia function and dysfunction. Annu Rev Neurosci *37*, 117-135. 10.1146/annurev-neuro-071013-013916.
9. Cui, G., Jun, S.B., Jin, X., Pham, M.D., Vogel, S.S., Lovinger, D.M., and Costa, R.M. (2013). Concurrent activation of striatal direct and indirect pathways during action initiation. Nature *494*, 238-242. 10.1038/nature11846.

10. Barbera, G., Liang, B., Zhang, L., Gerfen, C.R., Culurciello, E., Chen, R., Li, Y., and Lin, D.T. (2016). Spatially Compact Neural Clusters in the Dorsal Striatum Encode Locomotion Relevant Information. Neuron *92*, 202-213. 10.1016/j.neuron.2016.08.037.
11. Parker, J.G., Marshall, J.D., Ahanonu, B., Wu, Y.W., Kim, T.H., Grewe, B.F., Zhang, Y., Li, J.Z., Ding, J.B., Ehlers, M.D., and Schnitzer, M.J. (2018). Diametric neural ensemble dynamics in parkinsonian and dyskinetic states. Nature *557*, 177-182. 10.1038/s41586-018-0090-6.
12. Klaus, A., Martins, G.J., Paixao, V.B., Zhou, P., Paninski, L., and Costa, R.M. (2017). The Spatiotemporal Organization of the Striatum Encodes Action Space. Neuron *95*, 1171-1180 e1177. 10.1016/j.neuron.2017.08.015.
13. Yun, S., Yang, B., Anair, J.D., Martin, M.M., Fleps, S.W., Pamukcu, A., Yeh, N.H., Contractor, A., Kennedy, A., and Parker, J.G. (2023). Antipsychotic drug efficacy correlates with the modulation of D1 rather than D2 receptor-expressing striatal projection neurons. Nat Neurosci *26*, 1417-1428. 10.1038/s41593-023-01390-9.
14. Wilson, C.J., and Groves, P.M. (1981). Spontaneous firing patterns of identified spiny neurons in the rat neostriatum. Brain Res *220*, 67-80. 10.1016/0006-8993(81)90211-0.
15. Wilson, C.J., and Kawaguchi, Y. (1996). The origins of two-state spontaneous membrane potential fluctuations of neostriatal spiny neurons. J Neurosci *16*, 2397-2410. 10.1523/JNEUROSCI.16-07-02397.1996.
16. Guo, Q., Wang, D., He, X., Feng, Q., Lin, R., Xu, F., Fu, L., and Luo, M. (2015). Whole-brain mapping of inputs to projection neurons and cholinergic interneurons in the dorsal striatum. PLoS One *10*, e0123381. 10.1371/journal.pone.0123381.
17. Wall, N.R., De La Parra, M., Callaway, E.M., and Kreitzer, A.C. (2013). Differential innervation of direct- and indirect-pathway striatal projection neurons. Neuron *79*, 347-360. 10.1016/j.neuron.2013.05.014.
18. Wu, Y.W., Kim, J.I., Tawfik, V.L., Lalchandani, R.R., Scherrer, G., and Ding, J.B. (2015). Input- and cell-type-specific endocannabinoid-dependent LTD in the striatum. Cell Rep *10*, 75-87. 10.1016/j.celrep.2014.12.005.
19. Li, W., and Pozzo-Miller, L. (2020). Dysfunction of the corticostriatal pathway in autism spectrum disorders. J Neurosci Res *98*, 2130-2147. 10.1002/jnr.24560.
20. Surmeier, D.J., Plotkin, J., and Shen, W. (2009). Dopamine and synaptic plasticity in dorsal striatal circuits controlling action selection. Curr Opin Neurobiol *19*, 621-628. 10.1016/j.conb.2009.10.003.
21. Gerdeman, G.L., Ronesi, J., and Lovinger, D.M. (2002). Postsynaptic endocannabinoid release is critical to long-term depression in the striatum. Nat Neurosci *5*, 446-451. 10.1038/nn832.
22. Bagetta, V., Picconi, B., Marinucci, S., Sgobio, C., Pendolino, V., Ghiglieri, V., Fusco, F.R., Giampa, C., and Calabresi, P. (2011). Dopamine-dependent long-term depression is expressed in striatal spiny neurons of both direct and indirect pathways: implications for Parkinson's disease. J Neurosci *31*, 12513-12522. 10.1523/JNEUROSCI.2236-11.2011.

23. Kreitzer, A.C., and Malenka, R.C. (2007). Endocannabinoid-mediated rescue of striatal LTD and motor deficits in Parkinson's disease models. Nature *445*, 643-647. 10.1038/nature05506.
24. Marshall, J.J., Xu, J., and Contractor, A. (2018). Kainate Receptors Inhibit Glutamate Release Via Mobilization of Endocannabinoids in Striatal Direct Pathway Spiny Projection Neurons. J Neurosci *38*, 3901-3910. 10.1523/JNEUROSCI.1788-17.2018.
25. Chevaleyre, V., Takahashi, K.A., and Castillo, P.E. (2006). Endocannabinoid-mediated synaptic plasticity in the CNS. Annu Rev Neurosci *29*, 37-76. 10.1146/annurev.neuro.29.051605.112834.
26. Jackman, S.L., Chen, C.H., Chettih, S.N., Neufeld, S.Q., Drew, I.R., Agba, C.K., Flaquer, I., Stefano, A.N., Kennedy, T.J., Belinsky, J.E., et al. (2018). Silk Fibroin Films Facilitate Single-Step Targeted Expression of Optogenetic Proteins. Cell Rep *22*, 3351-3361. 10.1016/j.celrep.2018.02.081.
27. Aharoni, D., and Hoogland, T.M. (2019). Circuit Investigations With Open-Source Miniaturized Microscopes: Past, Present and Future. Front Cell Neurosci *13*, 141. 10.3389/fncel.2019.00141.
28. Shin, J.H., Song, M., Paik, S.B., and Jung, M.W. (2020). Spatial organization of functional clusters representing reward and movement information in the striatal direct and indirect pathways. Proc Natl Acad Sci U S A *117*, 27004-27015. 10.1073/pnas.2010361117.
29. Uchigashima, M., Narushima, M., Fukaya, M., Katona, I., Kano, M., and Watanabe, M. (2007). Subcellular arrangement of molecules for 2-arachidonoyl-glycerol-mediated retrograde signaling and its physiological contribution to synaptic modulation in the striatum. J Neurosci *27*, 3663-3676. 10.1523/JNEUROSCI.0448-07.2007.
30. Xu, J., Marshall, J.J., Kraniotis, S., Nomura, T., Zhu, Y., and Contractor, A. (2021). Genetic disruption of Grm5 causes complex alterations in motor activity, anxiety and social behaviors. Behav Brain Res *411*, 113378. 10.1016/j.bbr.2021.113378.
31. Conde-Ceide, S., Martinez-Viturro, C.M., Alcazar, J., Garcia-Barrantes, P.M., Lavreysen, H., Mackie, C., Vinson, P.N., Rook, J.M., Bridges, T.M., Daniels, J.S., et al. (2015). Discovery of VU0409551/JNJ-46778212: An mGlu5 Positive Allosteric Modulator Clinical Candidate Targeting Schizophrenia. ACS Med Chem Lett *6*, 716-720. 10.1021/acsmedchemlett.5b00181.
32. Xu, J., Zhu, Y., Contractor, A., and Heinemann, S.F. (2009). mGluR5 has a critical role in inhibitory learning. J Neurosci *29*, 3676-3684. 10.1523/JNEUROSCI.5716-08.2009.
33. Gerfen, C.R., Paletzki, R., and Heintz, N. (2013). GENSAT BAC cre-recombinase driver lines to study the functional organization of cerebral cortical and basal ganglia circuits. Neuron *80*, 1368-1383. 10.1016/j.neuron.2013.10.016.
34. Madisen, L., Zwingman, T.A., Sunkin, S.M., Oh, S.W., Zariwala, H.A., Gu, H., Ng, L.L., Palmiter, R.D., Hawrylycz, M.J., Jones, A.R., et al. (2010). A robust and high-throughput Cre reporting and characterization system for the whole mouse brain. Nat Neurosci *13*, 133-140. 10.1038/nn.2467.

35. Taverna, S., Ilijic, E., and Surmeier, D.J. (2008). Recurrent collateral connections of striatal medium spiny neurons are disrupted in models of Parkinson's disease. J Neurosci *28*, 5504-5512. 10.1523/JNEUROSCI.5493-07.2008.
36. Saunders, A., Johnson, C.A., and Sabatini, B.L. (2012). Novel recombinant adeno-associated viruses for Cre activated and inactivated transgene expression in neurons. Front Neural Circuits *6*, 47. 10.3389/fncir.2012.00047.
37. McElvain, L.E., Chen, Y., Moore, J.D., Brigidi, G.S., Bloodgood, B.L., Lim, B.K., Costa, R.M., and Kleinfeld, D. (2021). Specific populations of basal ganglia output neurons target distinct brain stem areas while collateralizing throughout the diencephalon. Neuron *109*, 1721-1738 e1724. 10.1016/j.neuron.2021.03.017.
38. Parent, A., and De Bellefeuille, L. (1982). Organization of efferent projections from the internal segment of globus pallidus in primate as revealed by fluorescence retrograde labeling method. Brain Res *245*, 201-213. 10.1016/0006-8993(82)90802-2.
39. Shen, W., Plotkin, J.L., Francardo, V., Ko, W.K., Xie, Z., Li, Q., Fieblinger, T., Wess, J., Neubig, R.R., Lindsley, C.W., et al. (2015). M4 Muscarinic Receptor Signaling Ameliorates Striatal Plasticity Deficits in Models of L-DOPA-Induced Dyskinesia. Neuron *88*, 762-773. 10.1016/j.neuron.2015.10.039.
40. Barnes, S.A., Pinto-Duarte, A., Kappe, A., Zembrzycki, A., Metzler, A., Mukamel, E.A., Lucero, J., Wang, X., Sejnowski, T.J., Markou, A., and Behrens, M.M. (2015). Disruption of mGluR5 in parvalbumin-positive interneurons induces core features of neurodevelopmental disorders. Mol Psychiatry *20*, 1161-1172. 10.1038/mp.2015.113.
41. Gong, S., Doughty, M., Harbaugh, C.R., Cummins, A., Hatten, M.E., Heintz, N., and Gerfen, C.R. (2007). Targeting Cre Recombinase to Specific Neuron Populations with Bacterial Artificial Chromosome Constructs. The Journal of Neuroscience *27*, 9817-9823.
42. Madisen, L., Zwingman, T.A., Sunkin, S.M., Oh, S.W., Zariwala, H.A., Gu, H., Ng, L.L., Palmiter, R.D., Hawrylycz, M.J., Jones, A.R., et al. (2010). A robust and high-throughput Cre reporting and characterization system for the whole mouse brain. Nature neuroscience *13*, 133-140. 10.1038/nn.2467.
43. Giovannucci, A., Friedrich, J., Gunn, P., Kalfon, J., Brown, B.L., Koay, S.A., Taxidis, J., Najafi, F., Gauthier, J.L., Zhou, P., et al. (2019). CaImAn an open source tool for scalable calcium imaging data analysis. Elife *8*. 10.7554/eLife.38173.
44. Zhou, P., Resendez, S.L., Rodriguez-Romaguera, J., Jimenez, J.C., Neufeld, S.Q., Giovannucci, A., Friedrich, J., Pnevmatikakis, E.A., Stuber, G.D., Hen, R., et al. (2018). Efficient and accurate extraction of in vivo calcium signals from microendoscopic video data. Elife *7*. 10.7554/eLife.28728.
45. Pennington, Z.T., Diego, K.S., Francisco, T.R., LaBanca, A.R., Lamsifer, S.I., Liobimova, O., Shuman, T., and Cai, D.J. (2021). ezTrack-A Step-by-Step Guide to Behavior Tracking. Curr Protoc *1*, e255. 10.1002/cpz1.255.
46. Edelstein, A.D., Tsuchida, M.A., Amodaj, N., Pinkard, H., Vale, R.D., and Stuurman, N. (2014). Advanced methods of microscope control using muManager software. J Biol Methods *1*. 10.14440/jbm.2014.36.

Acknowledgments

The authors thank Dr. Craig Weiss and Northwestern University behavioral phenotyping core facility for technical support.

Funding:

This work was supported by NIH R01 MH099114 to AC

Author contributions:

Conceptualization: JJM, JX, JGP, AC
Methodology: JJM, JX, JGP, AC
Investigation: JJM, JX, NHY, SY, TN, JA
Visualization: JJM, JGP, AC
Supervision: JJM, JGP, AC
Writing—original draft: JJM, AC
Writing—review & editing: JJM, AC, JGP

Competing interests:

The authors declare that they have no competing interests.

Data and materials availability:

All data needed to evaluate the conclusions in the paper are present in the paper and/or the Supplementary Materials. Code and summary data needed to replicate figures in the paper will be made publicly available in an archival database prior to the date of publication.

Figures legends:

Figure 1) dSPNs exhibit spatially clustered activity that varies with movement

(**A**) Cartoon representation of implanted GRIN lens and miniscope imaging in the DLS. (**B**) Examples of segmented cell outlines from the CNMF-E algorithm in a single mouse. (**C**) Example of Ca^{2+} traces from corresponding segmented cells shown in (B). (**D**) The probability of a Ca^{2+} event in detected cells increases during movement in dSPNs. (**E**) The Ca^{2+} event rate in detected cells increases during movement in dSPNs ($p=0.240$, Wilcoxon Signed Rank Test, events/second during bins with velocity>0.5 cm/sec vs. during bins with velocity<0.5 cm/sec). (**F**) Cartoon schematic to illustrate analysis of co-activity as a function of distance between cell pairs. Across all cell pairs in the field-of-view for each session, a correlation matrix was generated, in which, for each frame of the recording, the cell pair was scored a 1 if both cells were active, or 0 otherwise. These scores for each frame were averaged across all frames in the recording, to generate an average co-activity score for that pair. Then, those values were normalized to averages measured from independently shuffled Ca^{2+} traces for each cell in the recording (using 1000 independent shuffles for each cell trace), to control for changes in mean activity level between conditions. (**G**) Hypothetical plot of shuffle-normalized jaccard scores versus distance when coactivity is not “clustered” (**H**) Hypothetical plot of “clustered” co-activity. (**I**) dSPNs show “clustered” patterns of co-activity. (**J**) Co-activity decreases during periods of movement (Linear Mixed Effects Model/LMM, $p<0.000$, $z=-4.852$, $\beta=-1.671$, SE = 0.344, 95% CI: [-2.346 -0.996] , N=5 mice).

Figure 2) A negative allosteric modulator of mGluR5 increases clustered spatial coactivity among dSPN pairs

(**a**) Cartoon representing implanted GRIN lens and miniscope imaging in the DLS (**b**) Examples of segmented cell outlines from the CNMF-E algorithm in a single mouse. (**c**) Example of Ca^{2+} traces from corresponding segmented cells shown in (b) (**d**) Binned velocity of animal. Fenobam increased the amount of time the animal spends at rest (Vehicle mean: 0.324 ± 0.091, fenobam mean: 0.635 ± 0.043, $p=0.024$, $U=10$, Mann-

Whitney U test) (**e**) Mean velocity of animals following vehicle or fenobam treatment. The fenobam effect on mean velocity during the open field test is not significant (Mann-Whitney U test, p=0.103, U=48) (**f**) Mean bout length of animals during vehicle or fenobam. Fenobam reduces the mean bout length (Vehicle: 7.098 seconds ± 1.272, Fenobam: 2.886 seconds ± 0.160, Mann-Whitney U test, p<0.001, U=0), but does not affect the number of bouts (Mann-Whitney U test, p=0.793, U=35). (**g**) The average event rate of dSPNs at each movement velocity of the mouse. This relationship is not affected by fenobam administration (Linear Mixed Effects Model/LMM, p=0.754, z=-0.313, β=-0.002, SE = 0.006, 95% CI: [-0.014 0.010] , N=8 mice). (**h**) Fenobam increases the pairwise coactivity of dSPNs when grouped into 50 µm bins (LMM, p<0.000, z=-6.050, β=-0.828, SE = 0.137, 95% CI: [-1.096 -0.560] , N=8 mice) (**i**) Fenobam significantly increases coactivity of neuron pairs grouped into distal (275 µm - 500 µm) (Mann-Whitney U Test, p value=0.008, U=8) and proximal bins (50 µm - 275 µm) (Mann-Whitney U Test, p value=0.024, U=10). (**j**) Pairwise coactivity during rest with vehicle and fenobam treatment (velocity <0.5 cm*sec^{-1})(LMM, p<0.000, z=-4.448, β=-1.292, SE = 0.290, 95% CI: [-1.861 -0.723] , N=8 mice) (**k**) Pairwise coactivity during movement (velocity >0.5 cm*sec^{-1}) with vehicle and fenobam (LMM, p=0.008, z=-2.673, β=-0.220, SE = 0.082, 95% CI: [-0.381 -0.059] , N=8 mice) (**l**) Fenobam does not affect the relative decrease in coactivity seen during movement

Figure 3) Positive allosteric modulator of mGluR5, JNJ-46778212, decreases clustered coactivity of dSPNs

(**a**) Time animal spent in each velocity bin and (**b**) Mean velocity of the animals during vehicle and after JNJ administration. JNJ decreases the amount of time the animal spends at rest (Vehicle mean: 0.661 ± 0.066, JNJ mean: 0.294 ± 0.041, p=0.012, U=25, Mann-Whitney U test), however the change in mean velocity (**b**) is not significant (p=0.060, U=3, Mann-Whitney U test), nor is the mean bout length during vehicle and JNJ (p=0.060, U=3, Mann-Whitney U test) (**d**) Comparison of mean number of bouts of each animal during vehicle and JNJ (p=0.403, U=8, Mann-Whitney U test). (**e**) Mean event rate of Ca^{2+} transients in dSPNs during movement. JNJ administration does not significantly affect the event rate in dSPNs (LMM, p=0.058, z=1.893, β=0.010, SE =

0.005, 95% CI: [-0.000 0.020], N=4 mice) (**f**) Coactivity of pairs of dSPNs (50 µm bins) during total time in open field. Systemic JNJ administration reduces pairwise coactivity (LMM, p=0.003, z=2.964, β=-0.450, SE = 0.152, 95% CI: [-0.153 0.748], N=4 mice) (**g**) Cartoon showing pairwise coactivity analysis (**h**) Pairwise coactivity binned by 250 µm distance (proximal < 250 µm, distal > 250 µm). JNJ administration reduces pairwise coactivity in distal (Mann-Whitney U test, p=0.021, U=16) and proximal neuron pairs (Mann-Whitney U test, p=0.030, U=16). Normalized co-activity of dSPNs during rest. JNJ produces a small but significant reduction in coactivity measured during rest (velocity < 0.5 $cm*sec^{-1}$)(LMM, p=0.030, z=2.165, β=0.618, SE = 0.285, 95% CI : [0.059 1.177] , N=4 mice) (**j**) Normalized co-activity of dSPNs during movement (velocity > 0.5 $cm*sec^{-1}$). JNJ had a significant effect on dSPN clustered activity (LMM, p=0.027, z=-2.212, β=-1.694, SE = 0.766, 95% CI: [-3.195 -0.193], N=4 mice).(**k**) Event rate in dSPNs during vehicle and after JZL administration. JZL-184 administration reduces the event rate (LMM, p=0.001, z=3.195, β=0.007, SE = 0.002, 95% CI: [0.003 0.012] , N=5 mice) (**l**) Normalized co-activity of dSPNs against Euclidean distance. JZL had no effect on coactivity (LMM, p=0.065, z=-1.847, β=-1.204, SE = 0.652, 95% CI: [-2.481 0.074] , N=5 mice) (**m**) Time animals spent in velocity bins. JZL did not affect time spent at rest (p=0.531, U=16, Mann-Whitney U test).

Figure 4) mGluR5 cKO in Drd1a-expressing neurons reduces spontaneous motor behaviors and affects synaptic properties of dSPNs

(**a**) (Top) Cartoon representation of the role of mGluR5 in mobilizing eCBs at corticostriatal synapses. (Bottom) Representative EPSCs recorded prior to and during DHPG in WT mice (**b**) Example time course of corticostriatal EPSCs recorded in dSPNs during application of 100 µM DHPG in slice from WT mice. (**c**) Grouped data of DHPG depression. D1 cKO mice lack DHPG induced synaptic depression (cKO normalized EPSC amplitude: 0.754 ± 0.082, Wilcoxon Signed Rank Test, p=0.018, W=2; WT normalized amplitude: 0.992 ± 0.992, Wilcoxon Signed Rank Test p=0.834, W=9). (**d**) Time course of activity in open field and (**e**) Total distance traveled by WT and cKO mice. D1 cKO mice have reduced activity in the open field, measured as distance

travelled over time and total distance travelled during a 30-minute open-field session (Mann-Whitney U Test, U=245, p<0.001, N = 16 WT, 17 cKO). (**f**) Digging time in WT and cKO mice. D1 cKO mice spend less time digging when placed into a novel home cage (Mann-Whitney U Test, U=51.5, p=0.008, N = 7 WT, 8 cKO). (**g**) Latency to fall in the accelerating rotarod test. dSPN cKO mice have consistently reduced latency during the accelerating rotarod test over 3 days, with 4 sessions per day (p=0.024, F=5.709, Two-way repeated measures ANOVA, N = 12 WT, 17 cKO). (**h**) Running distance per hour on wireless wheels placed in home cage over 7 days. (**i**) Total distance run per day during first 3 days and over 7 days. D1 cKO mice ran significantly less during the first 3 days of testing (Mann-Whitney U Test, U=173, p=0.049) (**j**) Example traces of voltage response to 200pA current injection in WT and cKO mice. (**k**) There is not significant difference in the input output curve for current injection and AP firing between genotypes (LMM, p=0.056, z=1.913, β=1.197, SE = 0.626, 95% CI: [-0.029 2.424], N=26 cells, WT, N=22 cells, cKO). (**l**) Example mEPSC recordings in dSPN from WT and D1 cKO mice (**m**) Average amplitude of mEPSCs and cumulative distribution of amplitudes in WT and D1 cKO mice. There is no difference in amplitudes in recordings from the two genotypes (WT AMP: 21.04 ± 1.71 pA, N=15, cKO AMP: 16.66 ± 1.12, N=8, Mann-Whitney U Test, U=86.5, p=0.093) (**n**) Average mEPSC frequency and cumulative interevent intervals in WT and D1 cKO animals. D1 cKO mice have increased mEPSC frequency (WT Hz: 1.920 ± 0.3319 pA, N=15, cKO Hz: 3.325 ± 0.525, N=8, Mann-Whitney U Test, U=27.5, p=0.039)

Figure 5) D1 cKO mice show cell autonomous increase in clustered coactivity in dSPNs

(**a**) Cartoon representation of miniscope imaging in the DLS (**b**) Example segmented image from cKO mice (**c**) Example Ca^{2+} activity traces from identified dSPNs in cKO mice (**d**) Mean event rate during movement in WT and cKO animals. The event rate in dSPN cKO mice is unchanged from WT (LMM, p=0.651, z=0.452, β=0.003, SE = 0.007, 95% CI: [-0.011 0.017] , N=9 wt, 6 cKO) (**e**) Coactivity of pairs of dSPNs (50 µm bins) in WT and cKO animals. D1 cKO mice have increased coactivity across all pairwise

distances (MLM, $p=0.021$, $z=2.305$, $\beta=3.989$, SE = 1.731, 95% CI : [0.597 7.382] , N=9 wt, 6 cKO) (**f**) iSPN event rate in D1 cKO and WT animals is unchanged (LMM, $p=0.310$, $z=1.016$, $\beta=0.017$, SE = 0.016, 95% CI: [-0.015 0.048], N=3 wt, 3 cKO) (**g**) Clustered coactivity of iSPNs in WT and D1 mGluR5 cKO animals is unaffected (LMM, $p=0.691$, $z=0.398$, $\beta=2.368$, SE = 5.953, 95% CI: [-9.300 14.035], N=3 wt, 3 cKO).

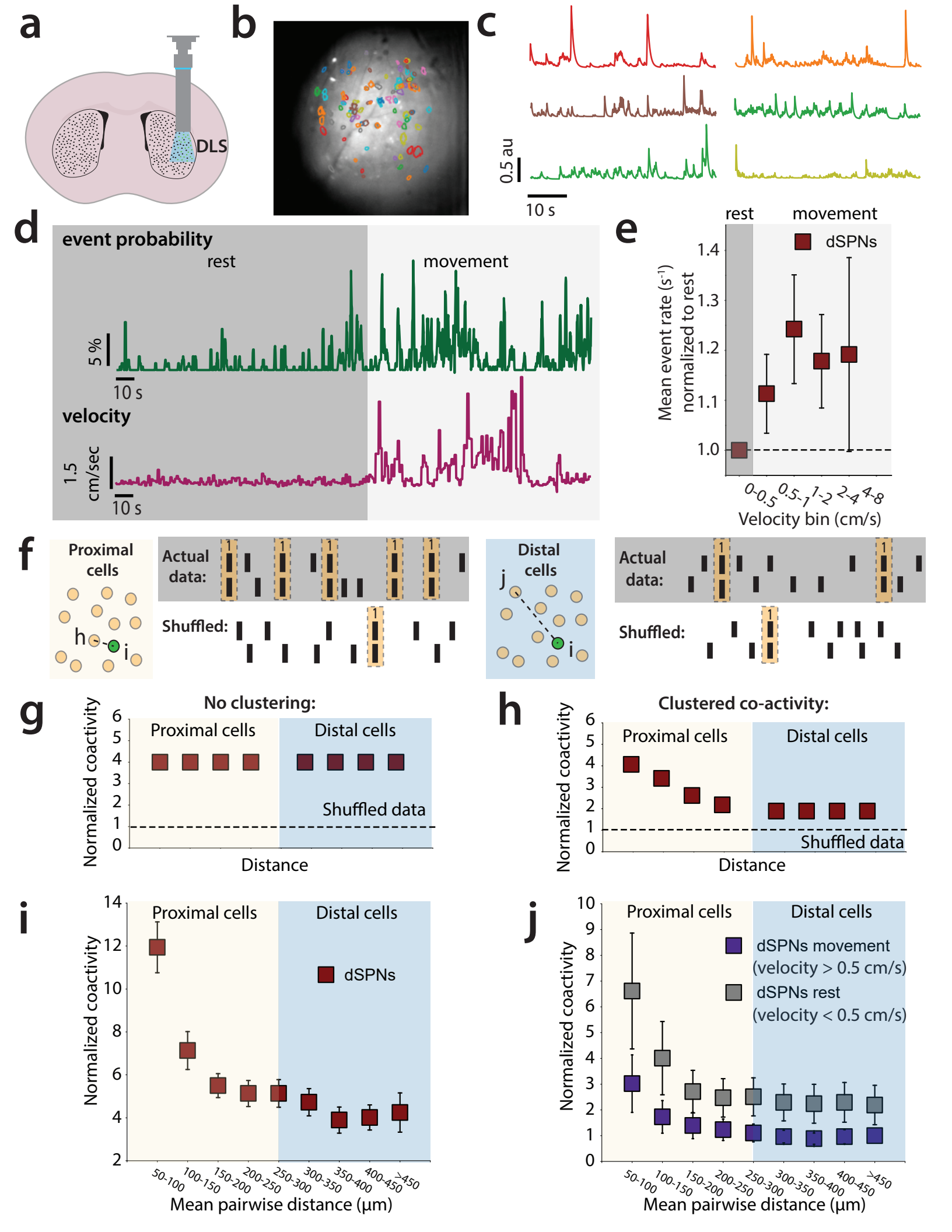
a
DLS
b
c
0.5 au
10 s
d
event probability
rest
movement
5 %
10 s
velocity
1.5 cm/sec
10 s
e
rest
movement
dSPNs
Mean event rate (s-1) normalized to rest
1.4
1.3
1.2
1.1
1.0
0-0.5
0.5-1
1-2
2-4
4-8
Velocity bin (cm/s)
f
Proximal cells
h
i
Actual data:
Shuffled:
Distal cells
j
i
Actual data:
Shuffled:
g
No clustering:
Normalized coactivity
Proximal cells
Distal cells
Shuffled data
Distance
h
Clustered co-activity:
Normalized coactivity
Proximal cells
Distal cells
Shuffled data
Distance
i
Normalized coactivity
Proximal cells
Distal cells
dSPNs
50-100
100-150
150-200
200-250
250-300
300-350
350-400
400-450
>450
Mean pairwise distance (μm)
j
Normalized coactivity
Proximal cells
Distal cells
dSPNs movement (velocity > 0.5 cm/s)
dSPNs rest (velocity < 0.5 cm/s)
50-100
100-150
150-200
200-250
250-300
300-350
350-400
400-450
>450
Mean pairwise distance (μm)

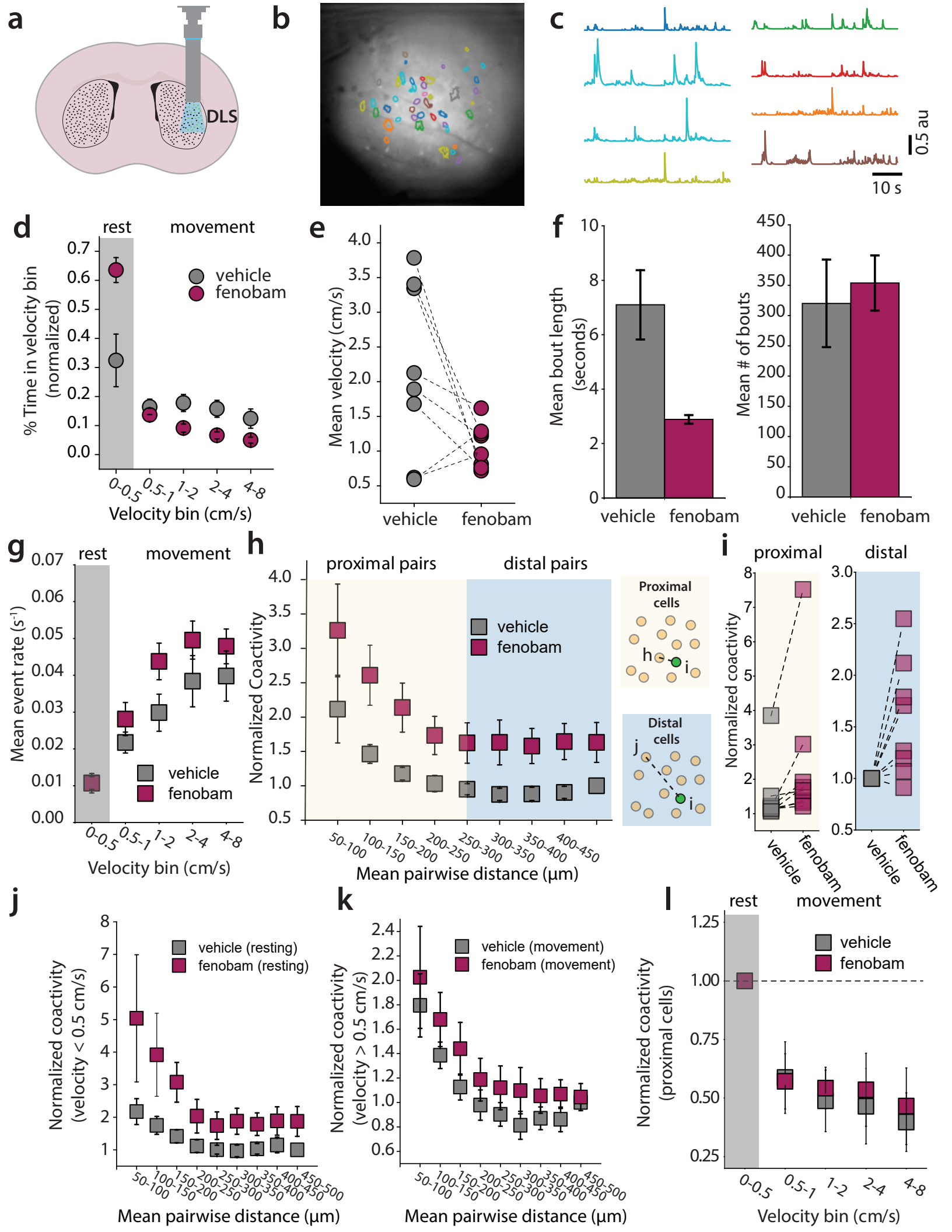
a
DLS
b
c
0.5 au
10 s
d
rest
movement
vehicle
fenobam
% Time in velocity bin (normalized)
0-0.5
0.5-1
1-2
2-4
4-8
Velocity bin (cm/s)
e
Mean velocity (cm/s)
vehicle
fenobam
f
Mean bout length (seconds)
Mean # of bouts
vehicle
fenobam
g
rest
movement
Mean event rate (s⁻¹)
vehicle
fenobam
Velocity bin (cm/s)
h
proximal pairs
distal pairs
vehicle
fenobam
Normalized Coactivity
Proximal cells
Distal cells
Mean pairwise distance (μm)
i
proximal
distal
Normalized coactivity
vehicle
fenobam
j
vehicle (resting)
fenobam (resting)
Normalized coactivity (velocity < 0.5 cm/s)
Mean pairwise distance (μm)
k
vehicle (movement)
fenobam (movement)
Normalized coactivity (velocity > 0.5 cm/s)
Mean pairwise distance (μm)
l
rest
movement
vehicle
fenobam
Normalized coactivity (proximal cells)
Velocity bin (cm/s)

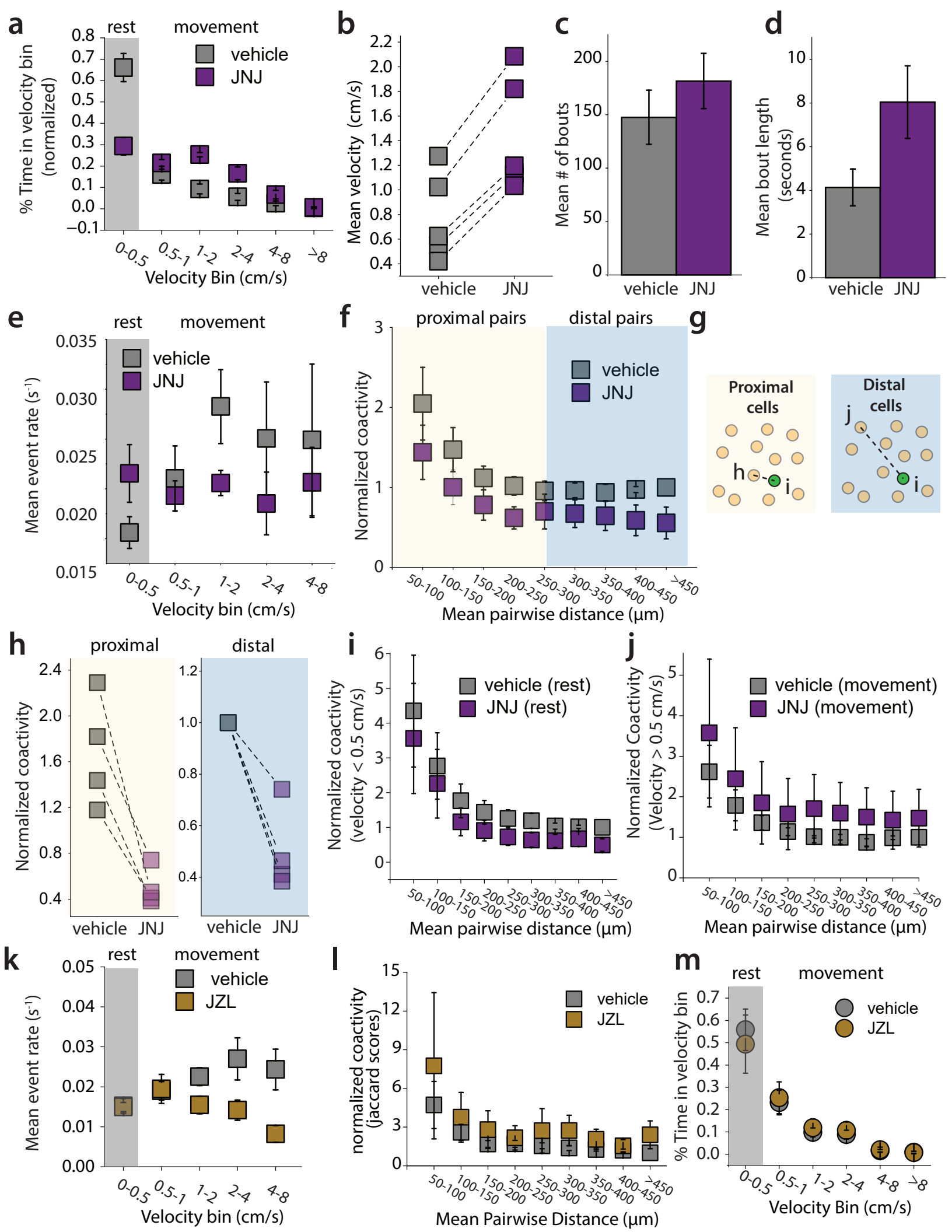
a
rest
movement
vehicle
JNJ
% Time in velocity bin (normalized)
0-0.5
0.5-1
1-2
2-4
4-8
>8
Velocity Bin (cm/s)
b
Mean velocity (cm/s)
vehicle
JNJ
c
Mean # of bouts
vehicle
JNJ
d
Mean bout length (seconds)
vehicle
JNJ
e
rest
movement
vehicle
JNJ
Mean event rate (s-1)
0-0.5
0.5-1
1-2
2-4
4-8
Velocity bin (cm/s)
f
proximal pairs
distal pairs
vehicle
JNJ
Normalized coactivity
50-100
100-150
150-200
200-250
250-300
300-350
350-400
400-450
>450
Mean pairwise distance (µm)
g
Proximal cells
h
i
Distal cells
j
i
h
proximal
distal
Normalized coactivity
vehicle
JNJ
vehicle
JNJ
i
vehicle (rest)
JNJ (rest)
Normalized coactivity (velocity < 0.5 cm/s)
50-100
100-150
150-200
200-250
250-300
300-350
350-400
400-450
>450
Mean pairwise distance (µm)
j
vehicle (movement)
JNJ (movement)
Normalized Coactivity (Velocity > 0.5 cm/s)
50-100
100-150
150-200
200-250
250-300
300-350
350-400
400-450
>450
Mean pairwise distance (µm)
k
rest
movement
vehicle
JZL
Mean event rate (s-1)
0-0.5
0.5-1
1-2
2-4
4-8
Velocity bin (cm/s)
l
vehicle
JZL
normalized coactivity (jaccard scores)
50-100
100-150
150-200
200-250
250-300
300-350
350-400
400-450
>450
Mean Pairwise Distance (µm)
m
rest
movement
vehicle
JZL
% Time in velocity bin
0-0.5
0.5-1
1-2
2-4
4-8
>8
Velocity Bin (cm/s)

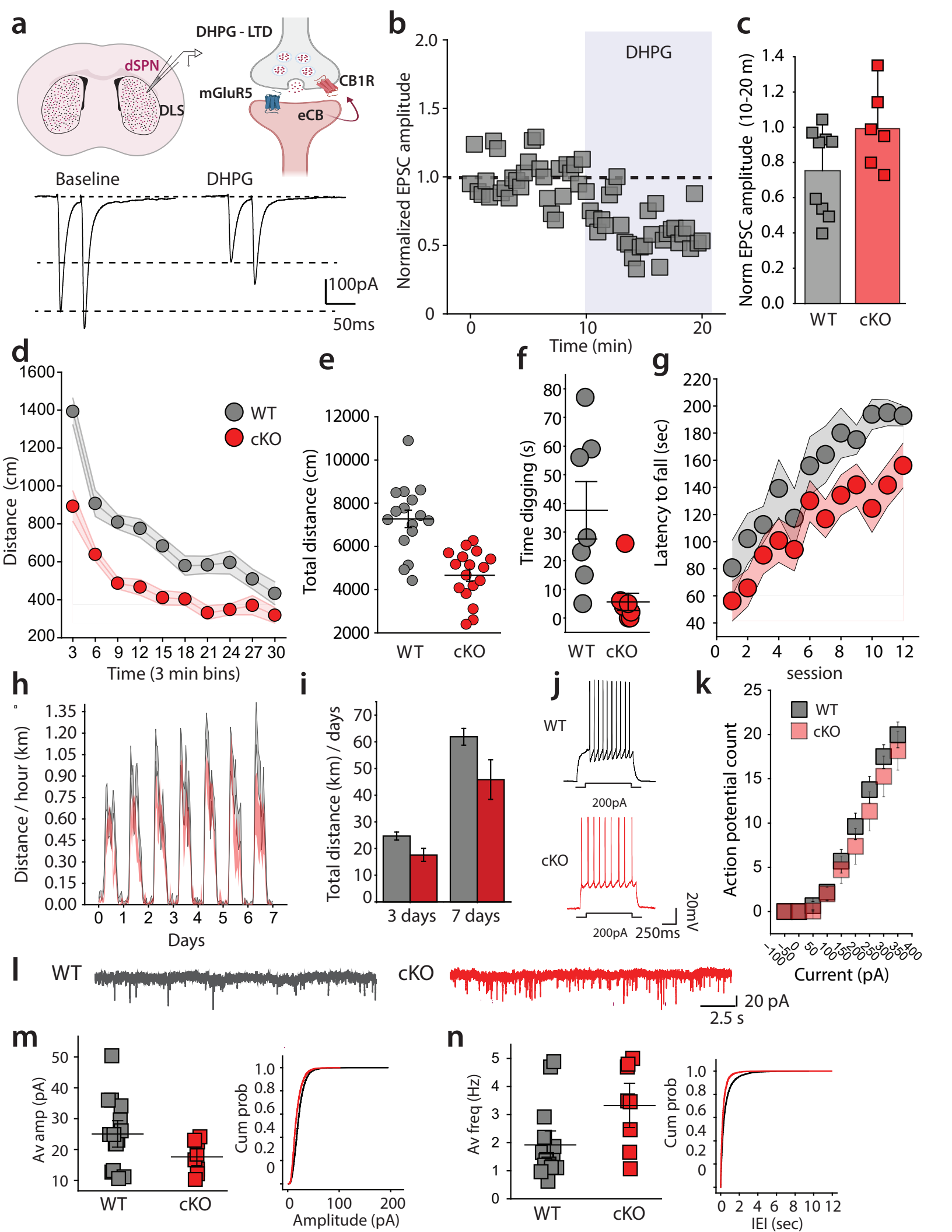
a
DHPG - LTD
dSPN
DLS
mGluR5
CB1R
eCB
Baseline
DHPG
100pA
50ms
b
DHPG
Normalized EPSC amplitude
Time (min)
c
Norm EPSC amplitude (10-20 m)
WT
cKO
d
WT
cKO
Distance (cm)
Time (3 min bins)
e
Total distance (cm)
WT
cKO
f
Time digging (s)
WT
cKO
g
Latency to fall (sec)
session
h
Distance / hour (km)
Days
i
Total distance (km) / days
3 days
7 days
j
WT
200pA
cKO
200pA
250ms
20mV
k
WT
cKO
Action potential count
Current (pA)
l
WT
cKO
20 pA
2.5 s
m
Av amp (pA)
WT
cKO
Cum prob
Amplitude (pA)
n
Av freq (Hz)
WT
cKO
Cum prob
IEI (sec)

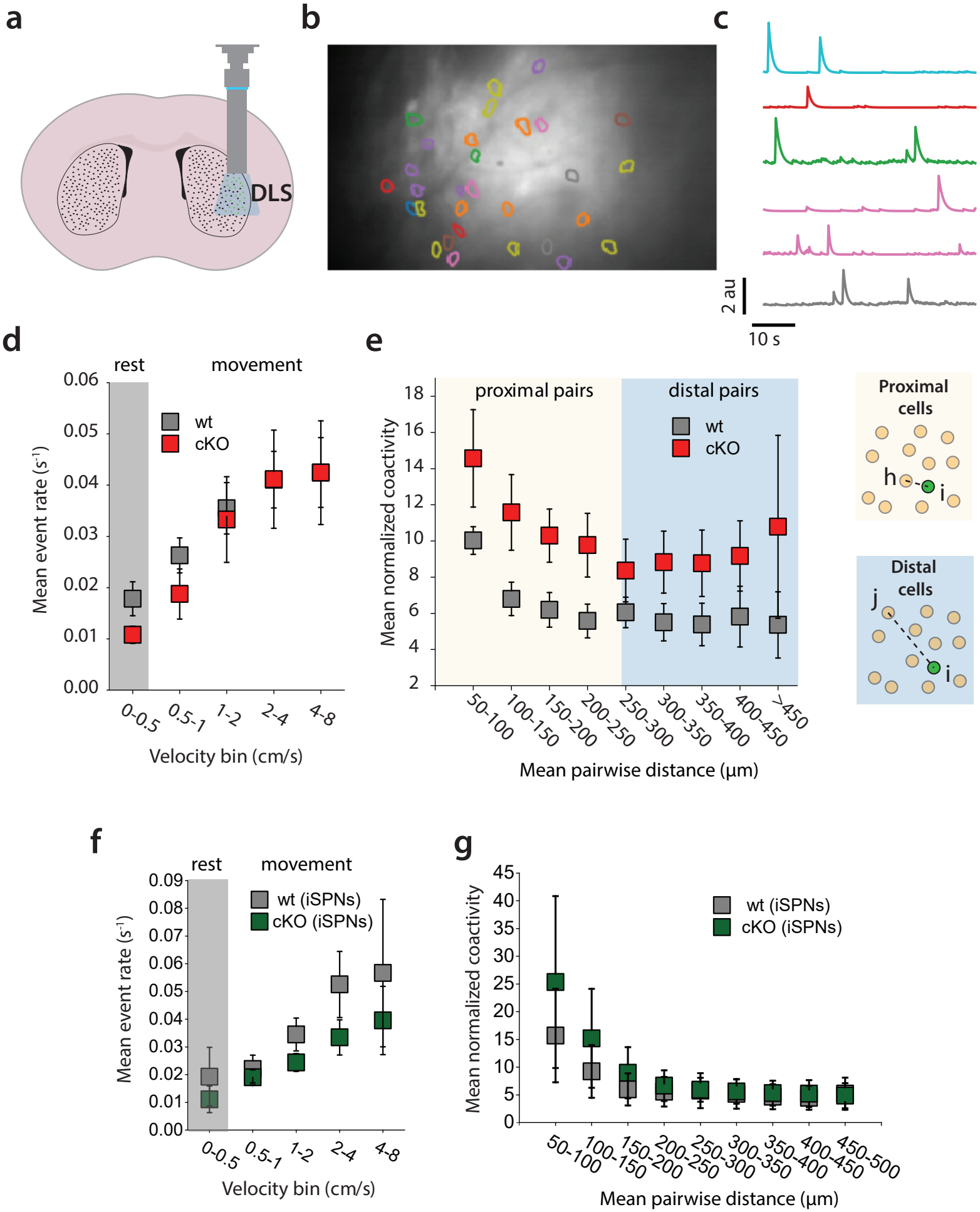
a
DLS
b
c
2 au
10 s
d
rest
movement
wt
cKO
Mean event rate (s-1)
0.06
0.05
0.04
0.03
0.02
0.01
0.00
0-0.5
0.5-1
1-2
2-4
4-8
Velocity bin (cm/s)
e
proximal pairs
distal pairs
wt
cKO
Mean normalized coactivity
18
16
14
12
10
8
6
4
2
50-100
100-150
150-200
200-250
250-300
300-350
350-400
400-450
>450
Mean pairwise distance (µm)
Proximal cells
h
i
Distal cells
j
i
f
rest
movement
wt (iSPNs)
cKO (iSPNs)
Mean event rate (s-1)
0.09
0.08
0.07
0.06
0.05
0.04
0.03
0.02
0.01
0.00
0-0.5
0.5-1
1-2
2-4
4-8
Velocity bin (cm/s)
g
wt (iSPNs)
cKO (iSPNs)
Mean normalized coactivity
45
40
35
30
25
20
15
10
5
0
50-100
100-150
150-200
200-250
250-300
300-350
350-400
400-450
450-500
Mean pairwise distance (µm)